Stability, Oxidation and Shape Evolution of PVP-Capped Pd Nanocrystals

Gillian Collins[†,‡], Michael Schmidt[†,‡], Gerard P. McGlacken[†], Colm O'Dwyer[†,§]

and Justin D. Holmes[†,‡,*]

[†]*Department of Chemistry and the Tyndall National Institute, University College Cork, Cork, Ireland.*

[‡]*Centre for Research on Adaptive Nanostructures and Nanodevices, Trinity College, Dublin, Ireland*

[§]*Materials and Surface Science Institute, University of Limerick, Limerick, Ireland.*

*To whom correspondence should be addressed: Tel: +353 (0)21 4903608; Fax: +353 (0)21 4274097; E-mail: j.holmes@ucc.ie

Abstract

A critical aspect in the practical application and enhanced catalytic performance of shape controlled nanocrystals is their stability and morphology retention under ambient conditions. Changes to the morphology of shape-controlled Pd nanocrystals capped by PVP are assessed by TEM and surface oxidation was evaluated by X-ray photoelectron spectroscopy (XPS), over 12 months. Surface oxidation of PVP-capped Pd nanocrystals resulted in loss of edge and corner sites and transition to spherical morphologies. The shape stability of the nanocrystals was found to follow the trend cubic < cuboctahedra < octahedral ~ concave cubes. For low index planes, {111} surfaces are more resistant to oxidation compared to {100} facets, correlating with the surface free energy of the nanocrystals. Cubic and cuboctahedral nanocrystals transitioned to spherical particles while octahedral nanocrystals retained their morphology. The presence of high energy {110} facets were observed in the cubic nanocrystals which undergo surface reconstruction. The presence of surface defects such as stacking faults were also found to influence the rate of the structural changes. Concave cubic nanocrystals, which possess high index facets and surface energies were consistently found to display excellent morphology retention. The concave cubic

nanocrystals displayed superior shape stability and reduced oxidation compared to cubic and cuboctahedral nanocrystals. XPS analysis further determined that PVP capping ligands on different Pd surface facets strongly influences the morphological consistency. The stability of the concave cubes can be attributed to stronger chemisorption of PVP capping ligands to the high index plane making them less susceptible to oxidation.

Keywords: Palladium, shape controlled nanocrystals, oxidation, stability, surface facet.

Introduction

Extensive developments in the controlled synthesis of noble metal nanocrystals (NCs), with specific morphologies, have allowed numerous shape-dependent properties to be determined.[1-3] Altering the morphology of a NC exposes surface facets which display different atomic arrangements, leading to applications in selective catalysis; several hydrogenation[4,5] and oxidation[6,7] reactions demonstrate facet dependent reactivity. Nanocrystal shape can also influence the optical properties of plasmonic nanostructures leading to enhanced sensing and biomedical applications.[8,9] While early research efforts focused on synthesizing NCs enclosed by low index surface facets, such as {111} and {100} surfaces, there has been enormous recent progress in the growth of NCs enclosed by high index faces, achieved by manipulating growth kinetics.[10,11] High-index facets are denoted by a set of Miller indices {*hkl*} with at least one index being greater than one. The morphologies of such structures are often characterized by sharp corners giving rise to unique optical properties and improved surface enhanced Raman scattering.[11] High index surfaces have a high density of low co-ordinated atoms located at step, edge and kink sites, thus have potential for enhanced catalysis.[12] Improved catalytic and electrocatalytic performance of NCs terminated by high index facets has been demonstrated.[13-16]

Pd is an important noble metal central to heterogeneous catalysis for chemical synthesis[17], fuel cells[18] and hydrogen storage.[19] Recent developments in understanding the growth conditions and mechanisms that influence NC morphology has facilitated exceptional control over the solution synthesis of Pd NCs enclosed by well-defined facets. Shape control synthesis of Pd NCs has been reported using selective capping ligands[20-22], seeded growth[14,23-26], heteroexpitaxial growth[27-29] and electrochemical methods[16,30]. The use of shape controlled Pd NCs has been shown or has been shown in enhanced performance in catalysis[14,27] and cancer therapy.[6]

Many practical applications of NCs, such as catalysis, require a metal to be deposited on a support material. The stability of shape-defined Pd NCs on support materials over time has not been thoroughly evaluated and is of key importance in exploiting the structure dependent properties of NCs. Loss of NC shape and changes in chemical state, due to surface oxidation, can have an impact on catalytic reactivity, molecular adsorption and optical properties.

Here, we report the stability and shape evolution of faceted Pd NCs supported on activated carbon. Activated carbon is one of the most commonly used support materials due to its high surface area, inertness and low cost. In this article, the stability of shape-controlled Pd nanostructures including cubic, octahedral and cuboctahedral NCs are assessed by TEM and XPS. In addition to low index NCs, the stability of concave cubes enclosed by high index surface facets is also investigated. The concave cubes displayed excellent stability after immobilization and superior oxidation resistance compared to cubic and cuboctahedral NCs. Structural features present in the as-synthesized NCs, such as surface faceting and defects, influence the stability of the NCs. XPS was utilized to probe the changes to the NC oxidation

state and to understand the origin of the stability observed for high index surface facets. In this study, the chemisorption of PVP on the surface of Pd NCs enclosed by different surface facets was found to be important for NC stability and retention of their morphology.

Experimental

Pd NCs of different surface facets were prepared by the methods described by Xia and co-workers.[26] A variety of NC shapes and sizes were investigated including 10 nm and 20 nm Pd cubic, 28 nm cuboctahedra and octahedral NCs with an edge length of 21 nm. High index facet concave cubes were prepared from 10 nm cubic seeds, measuring ~20 nm across in length and 35 nm from corner-corner.[14] For the stability studies six batched of the each NC were prepared. Pd NCs were immobilized on activated carbon by stirring at room temperature overnight and collected by filtration. Immobilization of the NCs on carbon was evident from the color change of the solution which changed from dark brown to near-colorless. The morphological stabilities of the carbon supported NCs was carried out by preparing the samples on TEM grids. Samples for analysis were prepared in triplicate and were left in ambient conditions (air, ~20 ºC).

Materials Characterization

Microscopy. Scanning electron microscopy (SEM) images were obtained using a FEI DualBeam Helios NanoLab 600i high resolution SEM. Transmission electron microscopy (TEM) analysis was performed using a JEOL 2100 transmission electron microscope, operating at a voltage of 200 kV. Scanning transmission electron microscopy (STEM) was carried out on a FEI Titan TEM at an operating voltage of 300 kV.

X-Ray Photoelectron Spectroscopy (XPS). XPS spectra were collected on a KRATOS-AXIS-165 using a monochromatic Al Kα line (1486.6 eV) as the X-ray source. All spectra were collected at a take-off angle (Θ) of 90° to the surface normal. Spectra were referenced to the C 1s at a binding energy 284.8 eV and a Shirley background was applied. The C1s spectra were fitted to Gaussian (70 %) Lorentzian (30 %) profiles. The high resolution Pd 3d scans were fitted with asymmetric Gaussian-Lorentzian profiles. The relative ratio of the Pd 3d doublet was fixed during the fitting, while the full width at half maximum (fwhm) and peak position were allowed to vary within a reasonable range to obtain the best fit.

Results and Discussion

1. Structural Stability of Pd Nanocrystals

The as-synthesized cubic Pd cubes, shown in figure 1 (a) are largely characterized by six {100} surface facets. The cubic morphology is unaffected by the immobilization procedure onto activated carbon as shown by the STEM image in figure 1(b). Exposure of the immobilized cubes for 7 days revealed little change in the morphology of the NCs, while analysis of the same NCs after 3 months revealed that the morphology of the 10 nm cubes altered. The change in shape changes was also observed to vary within a same sample, with some NCs becoming truncated whilst others displayed more pronounced changes, such as becoming spherical (Supporting Information Figure S1). After 6 months, the cubic NCs were almost entirely spherical in shape, as shown in figure 1(c). High resolution TEM analysis of the NCs after 6 months revealed that many of the particles were defect-free single crystalline, while others contained stacking defects such as those shown figure 1(d). In contrast, the 20 nm diameter NCs showed a greater retention of their morphology over time, with a mixture of slight and heavily truncated cubes observed as shown by comparison of the NCs 1 week and 6 months after deposition (figure 1 (e)-(f)). Cubic NCs stored under inert conditions (N_2

filled gloved box) after immobilization also exhibited rounded corners, consistent with surface atom diffusion, but no transformation from a cubic to a spherical morphology was observed indicating that interaction with O_2 influences NC stability. PVP-protected cubic NCs used in this study exhibited considerably greater stability compare to ethylene glycol protected NCs. Xiong *et. al.*[31] reported that dried 50 nm diameter Pd cubes capped with ethylene glycol formed a nanocrystalline PdO shell, readily observed by TEM after ~8 days of ambient exposure. Additionally, they reported an inverse relationship between NC size and stability with smaller (8 nm) cubes displaying superior stability (up to 90 days), compared to 50 nm cubes. This increased stability with decreasing size was not observed for the PVP-capped NCs used in this study, which clearly revealed that 10 nm cubes were less stable and lost their cubic morphology compared to the 20 nm cubes. Furthermore, TEM analysis on the aged cubes (after becoming spherical) did not show the presence of a crystalline oxide shell, suggesting a low degree of oxide formation due to a better surface passivation by bulkier PVP compared to ethylene glycol. The presence of the surrounding carbon matrix and polymeric capping ligands on the nanocrystals in this study, obstruct direct imaging of ultra-thin oxide layers by TEM.

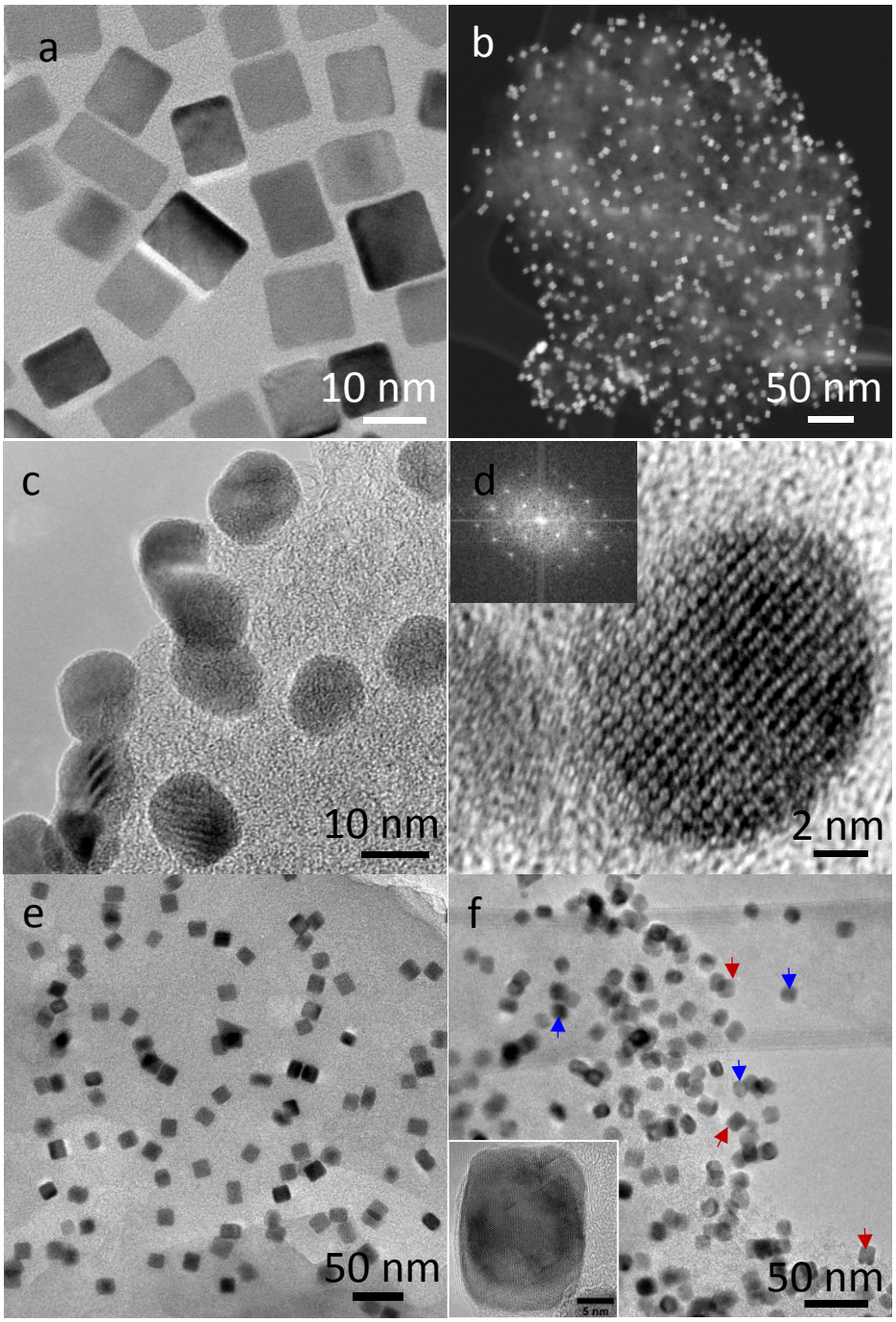

Figure 1. (a) TEM images of as-synthesized 10 nm PVP-capped cubic Pd NCs. (b) STEM image of 10 nm cubes deposited on activated carbon. (c) TEM image of 10 nm cubes 6 months after deposition onto carbon. (d) TEM image of cubic NC, aged for 12 months. (e) 20 nm cubic Pd NCs 1 week and (f) 6 months after deposition on activated carbon. The red arrows highlight NCs with well-maintained cubic morphologies and the blue arrows highlight

NCs evolved to truncated NCs. Figure (f) inset shows typical 20 nm cubic Pd NC 12 month after ambient exposure (scale bar is 5 nm).

The changes in the morphology of the Pd NCs from cubic to spherical are driven by energy minimization to the most thermodynamically favourable shape. To understand the factors contributing to the shape changes observed in the cubic NCs, high resolution TEM was used to analyze the particles at different stages of ageing. Figure 2(a) shows a TEM image of a freshly prepared cubic NC projected in the [011] direction. A significant feature shown in figure 2(a) is the presence of a {110} facet, which is not often observed on nanostructures due to its lower stability compared to {111} and {100} facets. The schematic shown in figure 2 illustrates the true structure of the cubic NCs showing the truncated corners with {111} and {110} facets in addition to the {100} cubic faces.[32] As shown in figure 2(a), these surfaces are relatively rough at the atomic scale and show missing-row reconstruction, characteristic of noble metal {110} surfaces.[33] In some regions, rows of atoms are missing along the [1-10] direction and give rise to a saw-tooth configuration, as identified by black arrows in figure 2(a). The image is magnified in the inset of figure 2(a) for clarity. Similar surface reconstruction has previously been observed on Au nanorods.[34] The presence of adatoms, shown by the white arrows in figure 2(a) is also observed. The driving force for this reconstruction is the formation of lower energy {111} micro facets on the (110) surface giving an overall lower surface energy after reconstruction, as illustrated by the inset schematic, in figure 2(a). No reconstruction was observed on the {100} facets and surface defects mainly consisted of single atom height terraces (Supporting Information Figure S2). A higher density of step sites was generally observed at the corners as shown in figure 2(b). Here, the presence of a higher index {220} and {310} facets can be seen where the {100} and {111} facets meet. This observation is in excellent agreement with DFT calculations

showing high index stepped surfaces being preferential to sharp corners at the boundaries between the (100) and (111) facets.[35] Additionally, as previously described, surface reconstruction of the {110} facets is again seen in figure 2(b). As the NCs age, loss of the stepped surfaces, which are more prevalent at the corners is observed, causing rounding of the corners (figure 2(c)). The facets continue to reduce in size, eventually becoming spherical (figure 2(d)). Such transformations are predicted by DFT calculations due to O_2 adsorption and surface oxide formation.[35] The presence of the {110} facet on the cubic NCs are influential to the stability of the NCs due to the greater reactivity and lower stability associated with the surface. Nanostructures with high surface defect densities are less stable and more susceptible to oxidation, thereby affecting the rate of structural changes.[36,37] Surface defects can also influence the co-ordination of capping ligands[38] and a more defective surface may disrupt the packing or lower the coverage of the PVP capping layer, facilitating easier oxidation of the Pd NCs.

An additional structural feature of the cubic NCs which contributes to their variable shape evolution is the presence of stacking faults, as shown in figure 2(c). Stacking faults were found to be present in some of the resulting spherical nanoparticles as shown in figure 2(f). The exact origin of the defects is unclear and was not investigated in detail in this study. The as-synthesized NCs are single crystalline with a low defect density, although stacking defects can be observed as shown in figure 2(c). Defect formation has been shown to occur as a stress relieve mechanism.[39]

The 20 nm cubic NCs display similar defect features to the 10 nm cubic NCs (figure 1(f) inset). The larger size of the particles may hinder complete transformation to spherical

morphology as the effects of surface stress and interface stress, are more pronounced for smaller particles.[40]

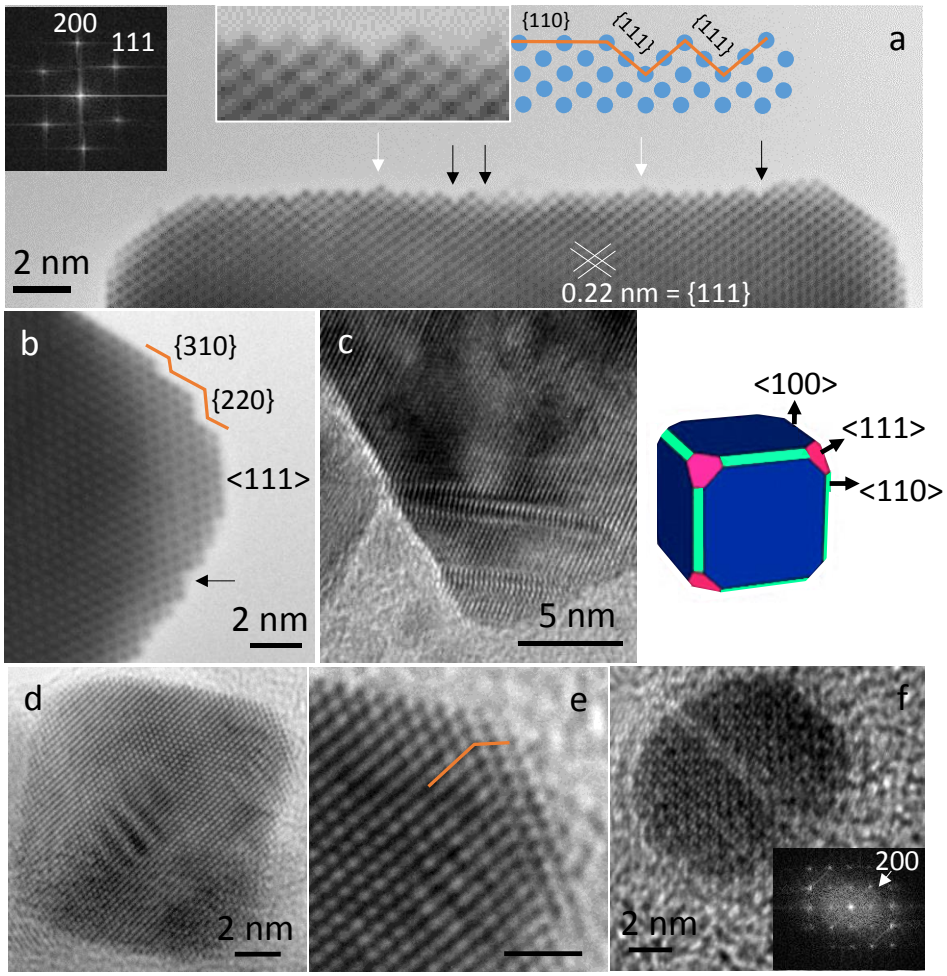

Figure 2. (a)-(b) HRTEM image of freshly synthesized cubic NC along the [110] direction. (c) Freshly prepared 20 nm cubic NC showing stacking faults. (d)-(e) 10 nm cubic NCs aged for 3 months and (f) cubic NC aged for 6 months showing stacking fault along the particle.

Pd NCs with a cuboctahedral morphology are characterized by 6 square {100} and 6 triangular {111} facets, shown in figure 3(a). Similar to the cubic NCs, aging of cuboctahedral NCs results in a morphology change to the thermodynamically lowest energy

spherical shape, as illustrated in figure 3(b). TEM also reveals that many of the NCs do not experience a uniform evolution of morphology. Figure 3(c) shows an aged octahedral NC with defined facets on one side of the NC and rounding on the opposite side of the NC, which was typical of many particles. The origin of the uneven rounding of surface facets is also attributed to the presence of surface defects as previous described for the cubic NCs. After 12 months many of the cuboctahedral NCs also became spherical (Supporting Information Figure S3).

In comparison to cubic and cuboctahedral NCs, the octahedral NCs exhibited little change to their morphology over the same time period. Ideal octahedra are characterized by eight {111} surface facets, however many of the octahedra prepared by this seeded method employed were slightly truncated, exposing vertices capped with {100} facets, as shown in the STEM image in figure 3(d). These NCs displayed excellent morphology retention as can be seen in figure 3(e), 6 months after deposition onto activated carbon. Even after 12 months the octahedral NCs displayed negligible changes to their morphology and the particles retained well-defined facets, see figure 3(f). The overall stability trend of the polyhedra was found to be cubic < cuboctahedra < octahedral, which correlates with the surface free energy of face centred cubic metals, $\gamma_{\{111\}} < \gamma_{\{100\}} < \gamma_{\{110\}}$.[41]

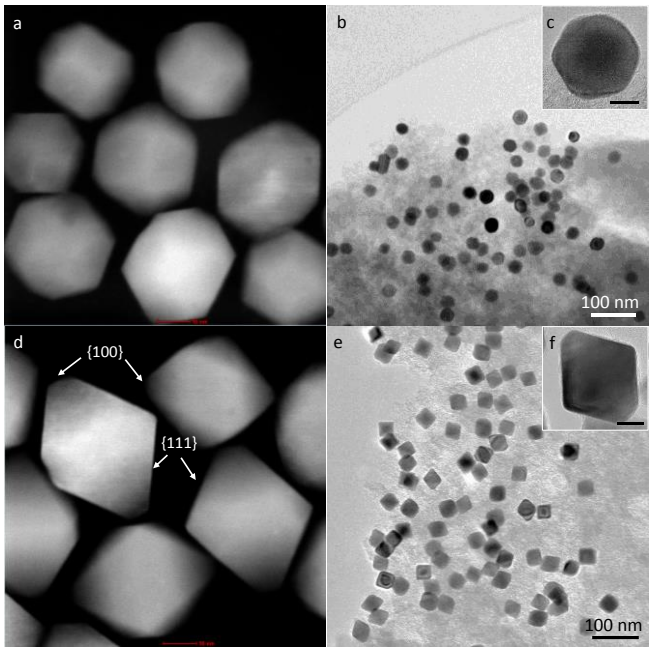

Figure 3. (a) STEM image of as-synthesized cuboctahedral NCs. (b)-(c) TEM image of cuboctahedral NCs 6 months after immobilization onto carbon. (d) STEM image of as-synthesized octahedral NCs. (e) Octahedral NCs 6 months and (f) 12 months after immobilization onto carbon. Scale bars in figures (a), (c), (d) and (f) are 10 nm.

High index surface facets are characterized by a high density of surface atoms with low coordination numbers. These open structures possess higher surface energies compared to closed pack surfaces, typically $\gamma_{\{111\}} < \gamma_{\{100\}} < \gamma_{\{hkl\}}$ for fcc Pd. Figure 4(a) shows a TEM image of as-synthesized concave Pd NCs. TEM analysis of the concave cubes 6 months after deposition on the carbon support revealed they exhibited excellent retention of morphology as shown in figure 4(b). In contrast to the cubic NCs, which loose the stepped facets on aging, HRTEM analysis of the concave cubes aged for 6 months (figure 4(c)) showed the preservation of the high index faces, with most of the exposed facets belonging to the {730} family planes, consistent with the as-synthesized NCs.[14] The NCs still retained their concave shape 12 month after deposition onto activated carbon (Supporting Information, Figure S4).

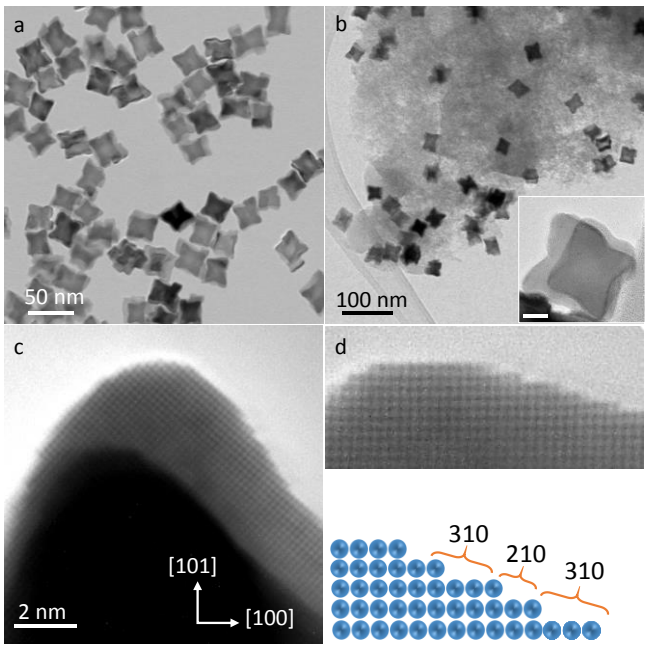

Figure 4. TEM image of (a) as synthesized concave NCs, (b) 6 months after deposited onto activated carbon. (d) HRTEM image of concave NC with incident beam along the [100] direction. The schematic illustrates the step configuration of the surface facet.

2. Oxidation and Interaction of PVP with Pd Nanocrystals

To further understand the stability of the shape-controlled NCs, XPS analysis was conducted to study the oxidation trends of the NCs as they aged and to probe the interaction of the PVP capping ligands with Pd. Figures 5(a)-(c) show the evolution of the Pd 3d core level spectra of the cubic Pd NCs over 24 h, 1 month and 6 months, respectively, after immobilization on activated carbon. The Pd 3d spectra of the cubic NCs after 24 h showed the presence of mainly metallic Pd(0) at a binding energy of 335.4 eV, in good agreement with bulk Pd (335.2 eV).[42] The slightly higher binding energy is typical of nanoparticles due to size and electronic effects.[43,44] Notably, assignment of Pd oxidation states in the 3d core level varies somewhat in literature. *In situ* XPS measurements of Pd(111) facets determined that peaks shifted to binding energies greater than +1.5 eV can be assigned to bulk oxide phases, while smaller shifts are attributed to surface oxide and sub-surface oxide species.[42,45] Similar

observations have been made for Pd(100) surfaces.[46,47] Stable surface oxides can form on (111) and (100) surfaces but not on (110) facets.[35,42] Furthermore, the structure of surface oxide species has been shown to be quite different from that of bulk PdO.[48] The second shoulder peak in figure 5(a), located at a binding energy of 337.1 eV can be assigned to bulk PdO, which is in excellent agreement with the 1.7 eV difference reported for PdO and Pd(0).[47,49] Exposure of 20 nm cubic NCs to ambient conditions for 1 month resulted in a similar Pd 3d spectra, but with increased line broadening of the peaks and a shift of 0.15 eV to higher binding energies, consistent with previous studies.[47,50] The first shoulder peak shown in figure 5(b) occurs at a binding energy of 336.5 eV, typical of PdO reported for nanoparticles.[50] The second shoulder peak centred at a binding energy of 337.6 eV, can typically be assigned to the presence of highly oxidized Pd species such as PdO_2 (reported in the range between 337.2 – 338.2 eV).[51-53] As the cubic NCs age over 6 months the PdO_x peak intensity increased, which can be seen from comparison of the Pd 3d spectra in figure 5(a)-(c). Figure 5(d) displays the Pd 3d spectra of concave cubes 4 weeks after immobilization onto activated carbon, showing the presence of predominately metallic Pd(0) at 335.2 eV and a surface PdO associated peak at 336.4 eV. Comparison of figures 5(c) and (e) clearly show that the concave cubes are considerably less oxidized than the cubic NCs after exposure to ambient conditions for 6 months, consistent with their shape retention. The total oxide signal for the concave cubes after 6 months was similar to that observed for {111} enclosed octahedral NCs, as shown in figures 5(e) and (f).

The nature of the surface facets present in the NCs is important for understanding the oxidation behaviour of faceted NCs. O_2 adsorption on Pd is spontaneous but absorption energies are facet dependent; Pd atoms on (110) surfaces have higher adsorption energies (1.56 eV/ O atom) compared to stepped or closed packed (111) or (100) surfaces.[35] The ease

of O_2 dissociation on Pd follows the trend {110} > {100} > {111}, which is the origin of the superior reactivity for oxidation-type reactions observed for Pd{110} catalysts.[6,54] Therefore, the {110} facets only observed on the cubic NCs are more reactive and susceptible to oxidation compared to the {111) and {100} facets, consistent with XPS observations.

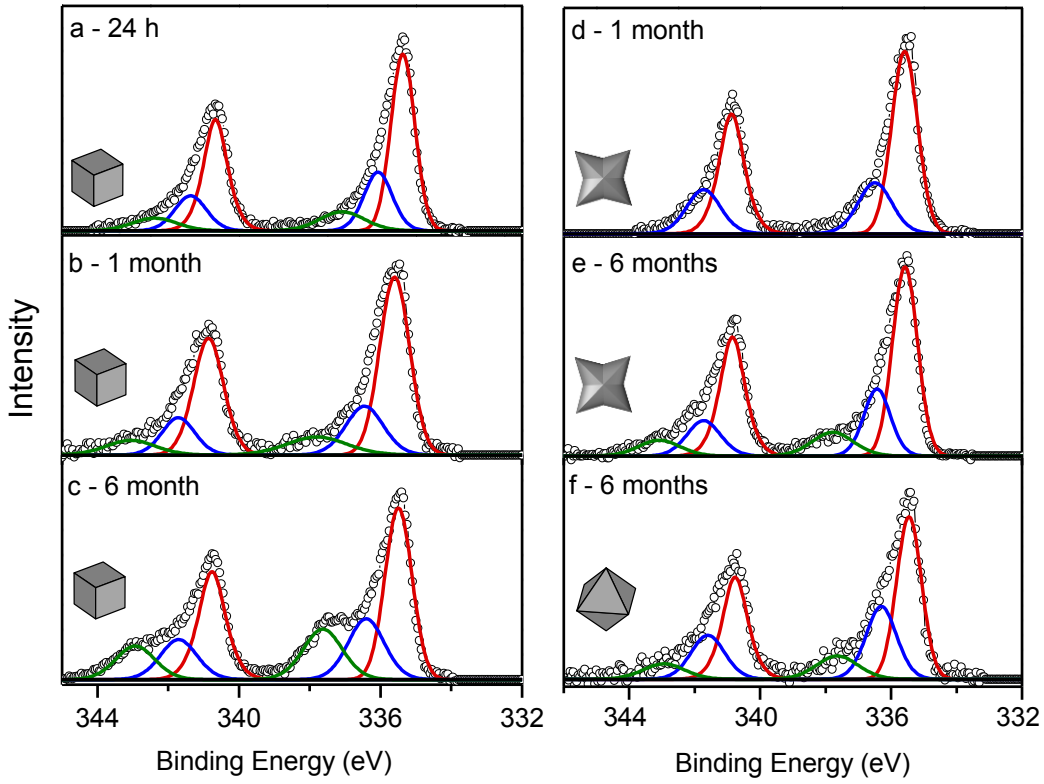

Figure 5. Background subtracted Pd 3d photoelectron emission spectra of carbon-supported Pd cubes after (a) 24 h, (b) 1 month (c) 6 months. Concave Pd cubes (d) 1 month, (e) 6 months and (f) octahedral NCs 6 months after ambient exposure.

The intriguing observation of this study is the excellent stability and oxidation resistance of concave NCs with high index facets, when the open structure of such facets is typically associated with high reactivity. Analysis of oxide phases on high index Pd surfaces is lacking in the literature. However, atomically smooth {100} and {111} surfaces have been suggested

to allow oxygen diffusion into the lattice, thereby destroying the surface structure and NC shape.[13,55] For low index surfaces, Pd(111) is more densely packed (1.53×10^{15} atoms cm^{-2}) compared to the Pd(100) surface (1.32×10^{15} atoms cm^{-2}) and Pd(110) surfaces (9.4×10^{14} atoms cm^{-2}). Consequently, oxide formation is the least favourable on Pd(111) as the higher surface atom density requires more lattice expansion to accommodate the formation of PdO_x.[56] Different factors may influence oxidation of high index surface. In contrast to low index planes, on high index faces, O_2 atoms preferentially adsorb at step sites rather than diffuse into the lattice, helping to preserve the surface structure.[13] The step structure of the high index facets may also better accommodate lattice strain induced by oxide formation, making them less susceptible to structural changes.

An important aspect in the stability of colloidal NCs is the presence of capping ligands at the particle surface. Passivating ligands can significantly alter surface free energy thereby influencing the stability and oxidation resistance of surface facets.[57] XPS analysis was used to investigate the interaction of PVP capping ligands with the Pd surface. Figure 6 shows the N 1s spectra of the different polyhedra. The cubic NCs displayed a single peak at a binding energy of 339.8 eV, characteristic of the pyrrolidone N group.[58] The N 1s binding energy is similar to that of the free PVP, indicating that the N atoms are not involved in the coordination with the Pd surface on cubic NCs, as illustrated in figure 6(b). In contrast to the cubic NCs, all other Pd polyhedra displayed the presence of a peak at 401.6 eV, in addition to the peak at 399.8 eV. Shifts to a higher binding energy are associated with decreased electron density of the N group, indicating charge transfer from the PVP to the Pd, implying that the pyrrolidone N group is involved in the coordination with the surface, as illustrated in figure 6(c). Xian *et al.*[58] showed the chemisorption of PVP to spherical Pd nanoparticles can also break the N-C bond in the N-C=O group, with following hydrolysis gave

$CH_2{-}CH_2{-}NH_2^+{-}(CH_2)_3{-}COO^-$, as illustrated in figure 6(d). Their report is in excellent agreement with the N 1s binding energy of 401.2 eV, observed here, which is generally assigned to protonated amine species.[59] The peak contribution of charged N species is larger for the concave cubes compared to the low index polyhedral, suggesting greater chemisorption of the pyrrolidone N group on the high index surface facets. The atomically stepped surface is characterized by low-coordinated number atoms which may facilitate a stronger interaction with the N groups. Bond cleavage is also considerably more favorable on stepped surfaces compared to atomically smooth surfaces which can lead to co-ordination of PVP as illustrated in figure 6(d).[60]

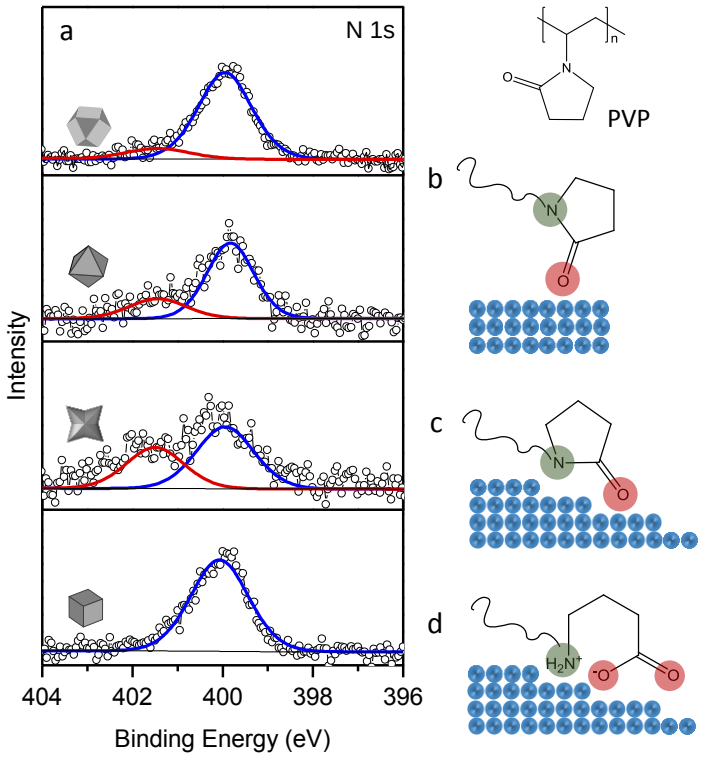

Figure 6. (a) N 1s spectra of Pd NCs immobilized on activated carbon. Schematic illustrating (b) the interaction of PVP through carbonyl O. (c) Co-ordination of PVP through both O and N groups. (d) Co-ordination of PVP with cleavage of the C-N bond.

The C 1s spectrum of the cubic Pd NCs, shown in figure 7(a) contains 3 components at binding energies of 284.8 eV (C-C, C=C), 286 eV (C-N, C-O) and 287.6 eV (C=O)[61], however adventitious hydrocarbon will also contribute to the C-C and C-O peak intensities. The C 1s spectrum of the concave cubes contains an additional peak not observed for the cubic NCs at a binding energy of 288.9 eV, typically assigned to the O-C=O group. The presence of the carboxylate group, in addition of the C=O group, indicates that a portion of the chemisorbed PVP molecules undergo cleavage of the C-N bond and subsequent hydrolysis, consistent with the N 1s spectrum. The synthesis of cubic NCs in this study uses Br^- ions as selective capping agents to promote the formation of NCs enclosed by {100} facets. Analysis of the Br 3d core level spectrum of the cubic NCs show that the Br^- species remain on the surface after immobilization onto activated carbon (Supporting Information Figure S5). The Pd(111) and high index facets were not observed to be capped with Br ions, which may facilitate stronger interactions with the PVP ligands compared to {100} facets. Furthermore, while Br ions have been shown to be chemisorbed to the surface, they can be displaced by ethylene glycol at 100 °C.[62] Removal of PVP from noble metal surfaces generally requires more forcing conditions.[63]

Several studies have shown that charge transfer and the co-ordination mode of PVP molecules with noble metal nanoparticles to be size dependent.[64-66] The XPS data in this study also indicates that the interaction mode of PVP capping ligands is also dependent on the nature of the surface facet for Pd NCs. This finding is important for both shape selective NC synthesis with high energy faceted surfaces, suggesting that the structure and electronic interaction of the ligand is important in preserving the long term stability and structure of high energy surfaces.

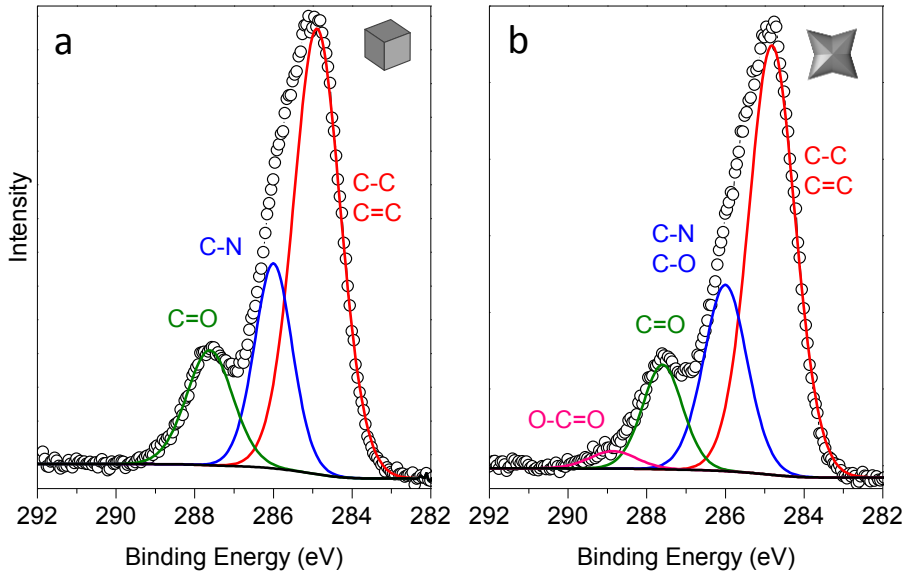

Figure 7. C 1s spectra of unsupported (deposited on glass substrate) (a) cubic Pd NCs and (b) concave cubic Pd NCs.

Conclusions

The stability, oxidation and shape evolution of well-defined Pd NCs supported on activated carbon was assessed over 12 months. For low index surfaces, the octahedral NCs with {111} facets had greater stability compared to {100} facets, due to the lower surface free energy. The presence of the relatively reactive and high energy {110} facet on the cubic NCs increases the oxidation susceptibility of the NCs making them the least stable shape studied. Surface defects influence the shape evolution of NCs resulting in non-uniform changes in their structure. Concave Pd NCs characterized by high index surface facets displayed superior stability to cubic and cuboctahedral NCs. XPS analysis identified stronger interaction between the N groups of the PVP capping ligands on the high index faces compared to the low index {100} facets. Controlling the interaction between the PVP capping ligands and the metal surface has been central in the synthesis of colloidal NCs. In particular understanding the selective chemisorption of capping ligands onto certain crystal

facets has been key to controlling the growth of NCs with specific morphologies. The work here highlights that these interactions also play a critical role in the long-term stability of NCs. Optimizing these interactions can facilitate the synthesis of NCs enclosed by well-defined surface facets with improved stability and oxidation resistance.

Structural evolution of nanoparticles is complex with several influencing factors. The stability trends observed in this study may not be general and nanoparticles prepared by alterative synthesis methods, with different capping ligands and support materials may display different stability trends. However, evaluating the stability of shape controlled nanocrystals is critical as morphological transformations due to surface defects or surface oxidation can influence the potential applications of shape-controlled such as catalysis. The excellent stability of PVP capped concaves cubes is promising as nanocrystals with high index facets have been shown to display enhanced reactivity in several catalytic applications.

Acknowledgments

We acknowledge financial support from Science Foundation Ireland (Grant 08/CE/I1432) and Enterprise Ireland (Grant IP/2011/0130). COD acknowledges the UCC Strategic Research Fund and an Irish Research Council New Foundations Award. The authors thank Dr. Fathima Laffir for assistance with XPS measurements.

Supporting Information

Additional TEM images of the cubic, cuboctahedral and concave cubic nanocrystals and the Br 3d core level XPS spectra for cubic nanocrystals can be found in the supporting information. This material is available free of charge via the Internet at http://pubs.acs.org.

References

(1) Xia, Y.; Xiong, Y.; Lim, B.; Skrabalak, S. E. Shape-Controlled Synthesis of Metal Nanocrystals: Simple Chemistry Meets Complex Physics? *Angew. Chem.-Int. Edit.,* **2009**, *48*, 60-103.

(2) Diaz Valenzuela, C.; Carriedo, G. A.; Valenzuela, M. L.; Zuniga, L.; O'Dwyer, C. Solid State Pathways to Complex Shape Evolution and Tunable Porosity during Metallic Crystal Growth. *Sci. Rep.,* **2013**, *3*.

(3) Niu, W.; Zhang, L.; Xu, G. Seed-Mediated Growth of Noble Metal Nanocrystals: Crystal Growth and Shape Control. *Nanoscale,* **2013**, *5*, 3172-3181.

(4) Bratlie, K. M.; Lee, H.; Komvopoulos, K.; Yang, P.; Somorjai, G. A. Platinum Nanoparticle Shape Effects on Benzene Hydrogenation Selectivity. *Nano Lett.,* **2007**, *7*, 3097-3101.

(5) Crespo-Quesada, M.; Yarulin, A.; Jin, M.; Xia, Y.; Kiwi-Minsker, L. Structure Sensitivity of Alkynol Hydrogenation on Shape- and Size-Controlled Palladium Nanocrystals: Which Sites Are Most Active and Selective? *J. Am. Chem. Soc.,* **2011**, *133*, 12787-12794.

(6) Long, R.; Mao, K.; Ye, X.; Yan, W.; Huang, Y.; Wang, J.; Fu, Y.; Wang, X.; Wu, X.; Xie, Y.et. al. Surface Facet of Palladium Nanocrystals: a Key Parameter to the Activation of Molecular Oxygen for Organic Catalysis and Cancer Treatment. *J. Am. Chem. Soc.,* **2013**, *135*, 3200-3207.

(7) Mostafa, S.; Behafarid, F.; Croy, J. R.; Ono, L. K.; Li, L.; Yang, J. C.; Frenkel, A. I.; Cuenya, B. R. Shape-Dependent Catalytic Properties of Pt Nanoparticles. *J. Am. Chem. Soc.,* **2010**, *132*, 15714-15719.

(8) Wiley, B. J.; Im, S. H.; Li, Z.-Y.; McLellan, J.; Siekkinen, A.; Xia, Y. Maneuvering the Surface Plasmon Resonance of Silver Nanostructures Through Shape-Controlled Synthesis. *J. Phys. Chem. B,* **2006**, *110*, 15666-15675.

(9) Zhang, J. Z. Biomedical Applications of Shape-Controlled Plasmonic Nanostructures: A Case Study of Hollow Gold Nanospheres for Photothermal Ablation Therapy of Cancer. *J. Phys. Chem. Lett.,* **2010**, *1*, 686-695.

(10) Quan, Z.; Wang, Y.; Fang, J. High-Index Faceted Noble Metal Nanocrystals. *Acc. Chem. Res.,* **2013**, *46*, 191-202.

(11) Hong, J. W.; Lee, S.-U.; Lee, Y. W.; Han, S. W. Hexoctahedral Au Nanocrystals with High-Index Facets and Their Optical and Surface-Enhanced Raman Scattering Properties. *J. Am. Chem. Soc.,* **2012**, *134*, 4565-4568.

(12) Xiong, Y.; Wiley, B. J.; Xia, Y. Nanocrystals with Unconventional Shapes - A Class of Promising Catalysts. *Angew. Chem. Int. Ed.,* **2007**, *46*, 7157-7159.

(13) Tian, N.; Zhou, Z.-Y.; Sun, S.-G.; Ding, Y.; Wang, Z. L. Synthesis of Tetrahexahedral Platinum Nanocrystals with High-Index Facets and High Electro-Oxidation Activity. *Science,* **2007**, *316*, 732-735.

(14) Jin, M.; Zhang, H.; Xie, Z.; Xia, Y. Palladium Concave Nanocubes with High-Index Facets and Their Enhanced Catalytic Properties. *Angew. Chem. Int. Ed.*

, **2011**, *50*, 7850-7854.

(15) Deng, Y.-J.; Tian, N.; Zhou, Z.-Y.; Huang, R.; Liu, Z.-L.; Xiao, J.; Sun, S.-G. Alloy Tetrahexahedral Pd-Pt Catalysts: Enhancing Significantly the Catalytic Activity by Synergy Effect of High-Index Facets and Electronic Structure. *Chem. Sci.,* **2012**, *3*, 1157-1161.

(16) Tian, N.; Zhou, Z.-Y.; Yu, N.-F.; Wang, L.-Y.; Sun, S.-G. Direct Electrodeposition of Tetrahexahedral Pd Nanocrystals with High-Index Facets and High Catalytic Activity for Ethanol Electrooxidation. *J. Am. Chem. Soc.,* **2010**, *132*, 7580-+.

(17) Blaser, H. U.; Indolese, A.; Schnyder, A.; Steiner, H.; Studer, M. Supported Palladium Catalysts for Fine Chemicals Synthesis. *J. Mol. Catal. A: Chem.,* **2001**, *173*, 3-18.

(18) Antolini, E. Palladium in Fuel Cell Catalysis. *Energy Environ. Sci.,* **2009**, *2*, 915-931.

(19) Kishore, S.; Nelson, J. A.; Adair, J. H.; Eklund, P. C. Hydrogen Storage in Spherical and Platelet Palladium Nanoparticles. *J. Alloys Compd.,* **2005**, *389*, 234-242.

(20) Xiong, Y. J.; McLellan, J. M.; Yin, Y. D.; Xia, Y. N. Synthesis of Palladium Icosahedra with Twinned Structure by Blocking Oxidative Etching with Citric Acid or Citrate Ions. *Angew. Chem. Int. Ed.,* **2007**, *46*, 790-794.

(21) Xiong, Y. J.; Xia, Y. N. Shape-Controlled Synthesis of Metal Nanostructures: The Case of Palladium. *Adv. Mater.,* **2007**, *19*, 3385-3391.

(22) Niu, Z.; Peng, Q.; Gong, M.; Rong, H.; Li, Y. Oleylamine-Mediated Shape Evolution of Palladium Nanocrystals. *Angew. Chem.-Int. Edit.,* **2011**, *50*, 6315-6319.

(23) Niu, W.; Li, Z.-Y.; Shi, L.; Liu, X.; Li, H.; Han, S.; Chen, J.; Xu, G. Seed-Mediated Growth of Nearly Monodisperse Palladium Nanocubes with Controllable Sizes. *Cryst. Growth Des.,* **2008**, *8*, 4440-4444.

(24) Zhang, Q.; Xie, J.; Yang, J.; Lee, J. Y. Monodisperse Icosahedral Ag, Au, and Pd Nanoparticles: Size Control Strategy and Superlattice Formation. *Acs Nano,* **2009**, *3*, 139-148.

(25) Niu, W.; Zhang, L.; Xu, G. Shape-Controlled Synthesis of Single-Crystalline Palladium Nanocrystals. *Acs Nano,* **2010**, *4*, 1987-1996.

(26) Jin, M.; Zhang, H.; Xie, Z.; Xia, Y. Palladium Nanocrystals Enclosed by {100} and {111} Facets in Controlled Proportions and their Catalytic Activities for Formic Acid Oxidation. *Energy Environ. Sci.,* **2012**, *5*, 6352-6357.

(27) Wang, F.; Li, C.; Sun, L.-D.; Wu, H.; Ming, T.; Wang, J.; Yu, J. C.; Yan, C.-H. Heteroepitaxial Growth of High-Index-Faceted Palladium Nanoshells and Their Catalytic Performance. *J. Am. Chem. Soc.,* **2011**, *133*, 1106-1111.

(28) Yu, Y.; Zhang, Q.; Liu, B.; Lee, J. Y. Synthesis of Nanocrystals with Variable High-Index Pd Facets through the Controlled Heteroepitaxial Growth of Trisoctahedral Au Templates. *J. Am. Chem. Soc.,* **2010**, *132*, 18258-18265.

(29) Fan, F.-R.; Liu, D.-Y.; Wu, Y.-F.; Duan, S.; Xie, Z.-X.; Jiang, Z.-Y.; Tian, Z.-Q. Epitaxial Growth of Heterogeneous Metal Nanocrystals: From Gold Nano-Octahedra to Palladium and Silver Nanocubes. *J. Am. Chem. Soc.,* **2008**, *130*, 6949-+.

(30) Tian, N.; Zhou, Z.-Y.; Sun, S.-G. Electrochemical Preparation of Pd Nanorods with High-Index Facets. *Chem. Comm.,* **2009**, 1502-1504.

(31) Xiong, Y. J.; Chen, J. Y.; Wiley, B.; Xia, Y. N.; Yin, Y. D.; Li, Z. Y. Size-Dependence of Surface Plasmon Resonance and Oxidation for Pd Nanocubes Synthesized via a Seed Etching Process. *Nano Lett.,* **2005**, *5*, 1237-1242.

(32) Xia, X.; Xie, S.; Liu, M.; Peng, H.-C.; Lu, N.; Wang, J.; Kim, M. J.; Xia, Y. On the Role of Surface Diffusion in Determining the Shape or Morphology of Noble-Metal Nanocrystals. *Proc. Natl. Acad. Sci. USA,* **2013**, *110*, 6669-6673.

(33) Bartynski, R. A.; Gustafsson, T. Experimental Study of Surface States on the (110) Faces of the Noble Metals. *Phys. Rev. B,* **1986**, *33*, 6588-6598.

(34) Wang, Z. L.; Gao, R. P.; Nikoobakht, B.; El-Sayed, M. A. Surface Reconstruction of the Unstable {110} Surface in Gold Nanorods. *J. Phys. Chem. B,* **2000**, *104*, 5417-5420.

(35) Mittendorfer, F.; Seriani, N.; Dubay, O.; Kresse, G. Morphology of Mesoscopic Rh and Pd Nanoparticles under Oxidizing Conditions. *Phys. Rev. B,* **2007**, *76*.

(36) Wang, Z. L. Transmission Electron Microscopy of Shape-Controlled Nanocrystals and their Assemblies. *J. Phys. Chem. B,* **2000**, *104*, 1153-1175.

(37) Gai, P. L.; Harmer, M. A. Surface Atomic Defect Structures and Growth of Gold Nanorods. *Nano Lett.,* **2002**, *2*, 771-774.

(38) Donkers, R. L.; Song, Y.; Murray, R. W. Substituent Effects on the Exchange Dynamics of Ligands on 1.6 nm Diameter Gold Nanoparticles. *Langmuir,* **2004**, *20*, 4703-4707.

(39) Ding, Y.; Fan, F.; Tian, Z.; L., W. W. Atomic Structure of Au-Pd Bimetallic Alloyed Nanoparticles. *J. Am. Chem. Soc.,* **2010**, *132*, 12480-12486.

(40) Jiang, Q.; Liang, L. H.; Zhao, D. S. Lattice Contraction and Surface Stress of fcc Nanocrystals. *J. Phys. Chem. B,* **2001**, *105*, 6275-6277.

(41) Barnard, A. S. Mapping the Shape and Phase of Palladium Nanocatalysts. *Catal. Sci. Technol.,* **2012**, *2*, 1485-1492.

(42) Lundgren, E.; Kresse, G.; Klein, C.; Borg, M.; Andersen, J. N.; De Santis, M.; Gauthier, Y.; Konvicka, C.; Schmid, M.; Varga, P. Two-dimensional oxide on Pd(111). *Phys. Rev. Lett.,* **2002**, *88*, 246103-246104.

(43) Smirnov, M. Y.; Vovk, E. I.; Kalinkin, A. V.; Pashis, A. V.; Bukhtiyarov, V. I. An XPS Study of the Oxidation of Noble Metal Particles Evaporated onto the Surface of an Oxide Support in Their Reaction with NOx. *Kinetics and Catalysis,* **2012**, *53*, 117-124.

(44) Paredis, K.; Ono, L. K.; Behafarid, F.; Zhang, Z.; Yang, J. C.; Frenkel, A. I.; Cuenya, B. R. Evolution of the Structure and Chemical State of Pd Nanoparticles during the in Situ Catalytic Reduction of NO with H-2. *J. Am. Chem. Soc.,* **2011**, *133*, 13455-13464.

(45) Ketteler, G.; Ogletree, D. F.; Bluhm, H.; Liu, H. J.; Hebenstreit, E. L. D.; Salmeron, M. In Situ Spectroscopic Study of the Oxidation and Reduction of Pd(111). *J. Am. Chem. Soc.,* **2005**, *127*, 18269-18273.

(46) Todorova, M.; Lundgren, E.; Blum, V.; Mikkelsen, A.; Gray, S.; Gustafson, J.; Borg, M.; Rogal, J.; Reuter, K.; Andersen, J. N.et. al. The Pd(100)-(root 5 x root 5)R27 degrees-O surface oxide revisited. *Surf. Sci.,* **2003**, *541*, 101-112.

(47) Wang, J.; Yun, Y.; Altman, E. I. The Plasma Oxidation of Pd(100). *Surf. Sci.,* **2007**, *601*, 3497-3505.

(48) Zemlyanov, D.; Aszalos-Kiss, B.; Kleimenov, E.; Teschner, D.; Zafeiratos, S.; Havecker, M.; Knop-Gericke, A.; Schlogl, R.; Gabasch, H.; Unterberger, W.et. al. In Situ XPS Study of Pd(111) Oxidation. Part 1: 2D Oxide Formation in 10^{-3} mbar O_2. *Surf. Sci.,* **2006**, *600*, 983-994.

(49) Peuckert, M. XPS Study on Surface and Bulk Pd Oxides, its Thermal Stability and a Comparison with Other Noble Metals. *J. Phys. Chem.,* **1985**, *89*, 2481-2486.

(50) Collins, G.; Blomker, M.; Osaik, M.; Holmes, J. D.; Bredol, M.; O'Dwyer, C. Three-Dimensionally Ordered Hierarchically Porous Tin Dioxide Inverse Opals and Immobilization of Palladium Nanoparticles for Catalytic Applications. *Chem. Mater.,* **2013**, *25*, 4312-4320.

(51) Kibis, L. S.; Stadnichenko, A. I.; Koscheev, S. V.; Zaikoyskii, V. I.; Boronin, A. I. Highly Oxidized Palladium Nanoparticles Comprising Pd4+ Species: Spectroscopic and Structural Aspects, Thermal Stability, and Reactivity. *J. Phys. Chem. C,* **2012**, *116*, 19342-19348.

(52) Kibis, L. S.; Titkov, A. I.; Stadnichenko, A. I.; Koscheev, S. V.; Boronin, A. I. X-Ray Photoelectron Spectroscopy Study of Pd Oxidation by RF Discharge in Oxygen. *Appl. Surf. Sci.,* **2009**, *255*, 9248-9254.

(53) Otto, K.; Haack, L. P.; Devries, J. E. Identification of Two Types of Oxidied Pd on Gamma Alumina by XPS. *Appl. Catal. B,* **1992**, *1*, 1-12.

(54) Wang, F.; Lu, Z.; Yang, L.; Zhang, Y.; Tang, Q.; Guo, Y.; Ma, X.; Yang, Z. Palladium Nanoparticles with High Energy Facets as a Key Factor in Dissociating O_2 in the Solvent-Free Selective Oxidation of Alcohols. *Chem. Commun.,* **2013**, *49*, 6626-6628.

(55) Leisenberger, F. P.; Koller, G.; Sock, M.; Surnev, S.; Ramsey, M. G.; Netzer, F. P.; Klotzer, B.; Hayek, K. Surface and Subsurface Oxygen on Pd(111). *Surf. Sci.,* **2000**, *445*, 380-393.

(56) Han, J. Kinetic and Morphological Studies of Palladium Oxidation in O_2-CH_4 Mixtures, Worcester Poltechnic Institute 2004.

(57) Collins, G.; Fleming, P.; Barth, S.; O'Dwyer, C.; Boland, J. J.; Morris, M. A.; Holmes, J. D. Alkane and Alkanethiol Passivation of Halogenated Ge Nanowires. *Chem. Mater.,* **2010**, *22*, 6370-6377.

(58) Xian, J. Y.; Hua, Q.; Jiang, Z. Q.; Ma, Y. S.; Huang, W. X. Size-Dependent Interaction of the Poly(N-vinyl-2-pyrrolidone) Capping Ligand with Pd Nanocrystals. *Langmuir,* **2012**, *28*, 6736-6741.

(59) Graf, N.; Yegen, E.; Gross, T.; Lippitz, A.; Weigel, W.; Krakert, S.; Terfort, A.; Unger, W. E. S. XPS and NEXAFS Studies of Aliphatic and Aromatic Amine Species on Functionalized Surfaces. *Surf. Sci.,* **2009**, *603*, 2849-2860.

(60) Klier, K.; Hess, J. S.; Herman, R. G. Structure Sensitivity of Methane Dissociation on Palladium Single Crystal Surfaces. *J. Chem. Phys.,* **1997**, *107*, 4033-4043.

(61) Truica-Marasescu, F.; Wertheimer, M. R. Nitrogen-Rich Plasma-Polymer Films for Biomedical Applications. *Plasma Processes Polym.,* **2008**, *5*, 44-57.

(62) Peng, H.-C.; Xie, S.; Park, J.; Xia, X.; Xia, Y. Quantitative Analysis of the Coverage Density of Br- Ions on Pd{100} Facets and Its Role in Controlling the Shape of Pd Nanocrystals. *J. Am. Chem. Soc.,* **2013**, *135*, 3780-3783.

(63) Nui, Z.; Li, Y. Removal and Utilization of Capping Agents in Nanocatalysis *Chem. Mater.,* **2014**, *26*, 72-83.

(64) Qiu, L. M.; Liu, F.; Zhao, L. Z.; Yang, W. S.; Yao, J. N. Evidence of a Unique Electron Donor-Acceptor Property for Platinum Nanoparticles as Studied by XPS. *Langmuir,* **2006**, *22*, 4480-4482.

(65) Xian, J.; Hua, Q.; Jiang, Z.; Ma, Y.; Huang, W. Size-Dependent Interaction of the Poly(N-vinyl-2-pyrrolidone) Capping Ligand with Pd Nanocrystals. *Langmuir,* **2012**, *28*, 6736-6741.

(66) Tsunoyama, H.; Ichikuni, N.; Sakurai, H.; Tsukuda, T. Effect of Electronic Structures of Au Clusters Stabilized by Poly(N-vinyl-2-pyrrolidone) on Aerobic Oxidation Catalysis. *J. Am. Chem. Soc.,* **2009**, *131*, 7086-7093.

TOC